frontiers | Frontiers in Marine Science

TYPE Original Research
PUBLISHED 23 January 2025
DOI 10.3389/fmars.2025.1489202

OPEN ACCESS

EDITED BY
Francisco Machín,
University of Las Palmas de Gran Canaria, Spain

REVIEWED BY
Chengjian Jiang,
Guangxi University of Science and Technology, China
Chongwei Peng,
Beibu Gulf University, China

*CORRESPONDENCE
Lingling Xie
xiell@gdou.edu.cn

RECEIVED 31 August 2024
ACCEPTED 02 January 2025
PUBLISHED 23 January 2025

CITATION
Zeng F, Xie L, Li M, Li Q and Liu S (2025) Seasonal variation of underwater sound propagation in the Beibu Gulf.
Front. Mar. Sci. 12:1489202.
doi: 10.3389/fmars.2025.1489202

Seasonal variation of underwater sound propagation in the Beibu Gulf

Feihong Zeng[1,2], Lingling Xie[1,2,3]*, Mingming Li[1,2,3], Qiang Li[1,2,3] and Simeng Liu[1,2]

[1]Laboratory of Coastal Ocean Variation and Disaster Prediction, College of Oceanology and Meteorology, Guangdong Ocean University, Zhanjiang, China, [2]Guangdong Key Laboratory of Climate, Resource and Environment in Continental Shelf Sea and Deep Ocean, Zhanjiang, China, [3]Key Laboratory of Spatial Ocean Remote Sensing and Application, Zhanjiang, China

Variations in the underwater sound speed significantly influence sound propagation in the ocean, thereby impacting both underwater navigation systems and a substantial portion of marine organisms reliant on sound. This study utilizes cruise data from the Beibu Gulf during the summer and winter of 2023–2024 to explore the seasonal variations in temperature and salinity affecting the sound speed distribution and characteristics of sound propagation. Results indicate significant differences in the sound speed on either side of the 30-m isobath in the Beibu Gulf, with pronounced changes corresponding to seasonal temperature and salinity variations. In summer, the sound speed in the Beibu Gulf exhibits a north-high–south-low pattern. In areas shallower than 30 m, the sonocline is predominantly positive or absent, whereas, in deeper areas, it is mainly negative. During winter, there is a south-high–north-low pattern in sound speed across the Beibu Gulf, with pronounced sound speed extremes in areas shallower than 30 m. Sound propagation simulations based on the Beibu Gulf sound-speed field reveal that sounds at the 100-Hz frequency propagate significantly farther and cover larger areas in depths less than 30 m compared to deeper areas. In summer, this phenomenon is more pronounced than in winter due to the presence of positive sonoclines. The results have significant implications for target detection, underwater acoustic communication, and the protection of aquatic animals that rely on underwater sound for survival in the Beibu Gulf.

KEYWORDS

seasonal variation, sound speed, underwater sound propagation, the Beibu Gulf, thermohaline

1 Introduction

Underwater sound propagation is a critical component of both maritime operations and ecological systems, especially in semi-enclosed water bodies like the Beibu Gulf. Positioned between 17° N–22°N and 105°E–110°E, the Beibu Gulf spans approximately 130,000 km² in the northwestern South China Sea (Johnston and Cain, 1982; Soloviev et al., 2009; Gao et al., 2017; Liu et al., 2021; Lunkov et al., 2021). This region experiences substantial shipping traffic and exploration activities and hosts a rich diversity of marine species. The gulf is characterized by an average depth of around 40 m, with most areas not exceeding 100 m in depth (Zheng et al., 2012; Xia et al., 2024; Yu et al., 2020; Koongolla et al., 2020).

Marine organisms in the Beibu Gulf rely heavily on sound for essential life functions, including communication, navigation, feeding, and reproduction (Au and Hastings, 2008; Hildebrand, 2009). However, anthropogenic activities, particularly shipping, introduce significant underwater noise pollution that potentially masks biological signals and alters the behaviors of marine animals. Such disturbances can have profound effects on the ecosystem. Previous research studies, including studies in similar environments like the semi-enclosed Red Sea, have used noise maps to assess the impact of ship traffic and provide insights into the effects of human-induced noise on marine life. These studies aid policymakers in crafting targeted mitigation strategies (Larayedh et al., 2024).

Despite extensive research into the thermohaline properties of the Beibu Gulf, their impacts on the underwater acoustic environment and sound propagation remain underexplored (Chen et al., 2011, 2015; Li et al., 2022). Few studies have employed reanalysis data to simulate underwater sound propagation (Ermolaev and Bui, 2014) and acoustic attenuation in sediments (Liu and Lu, 2008), and none have specifically analyzed variations in the acoustic environment of the Beibu Gulf. Notably, there is a gap in research concerning how seasonal temperature and salinity changes affect the sound-speed field, although seasonal variations in sound speed could significantly alter underwater sound propagation (Spiesberger et al., 1983).

The acoustic environment is influenced by factors such as sound speed, environmental boundaries, and water depth, which are intrinsically linked to the thermohaline characteristics of seawater (Lamarre and Melville, 1994; Li et al., 2021; Siderius and Porter, 2008; Wu et al., 2015). These factors display both spatial and seasonal variability, which may be further influenced by larger-scale oceanographic processes like the El Niño–Southern Oscillation or broader climate patterns, making them vital subjects in ocean acoustics research (Affatati et al., 2022; Liu et al., 2023; Klusek and Lisimenka, 2016). Moreover, climate change exacerbates these dynamics, with shifts in sea surface temperatures and salinity gradients, potentially affecting sound propagation and, consequently, marine life-dependent acoustic cues (Hildebrand, 2009).

Addressing these knowledge gaps and the growing importance of understanding climate change's impact on marine ecosystems, this study aims to (1) analyze changes in the sound-speed field resulting from seasonal temperature and salinity variations in the Beibu Gulf; (2) explore the seasonal variations of sound propagation across different source frequencies and emission angles; and (3) investigate the predominance of sound-speed fields in underwater sound propagation in the Beibu Gulf, along with their potential long-term implications for marine life and maritime operations.

2 Materials and methods

2.1 Cruise data

Three research cruises were conducted by Guangdong Ocean University in the Beibu Gulf, South China Sea, from 22 July to 10 August 2023, 9 to 18 December 2023, and 11 to 16 January 2024. During these cruises, 32 sections were surveyed across extensive areas of the Beibu Gulf to study its vertical structure and water properties in both summer and winter seasons, with 16 sections per season (Figure 1). Temperature and salinity profiles were measured at full depth with a vertical resolution of 1 m using three SBE19Plus conductivity–temperature–depth (CTD) instruments installed aboard the research vessels *Tianlong*, *Yuezhanyuke 6*, *Yuezhanyuyun-01018*, and *Leiyu-12086*. The SBE19Plus CTD instruments operate at a sampling frequency of 4 Hz, providing a temperature resolution of 0.0001°C and a conductivity resolution of 0.00005 S/m, with an accuracy of 0.005°C for temperature and 0.0005 S/m for conductivity.

In the CTD data collection process, we strictly follow the steps outlined below to ensure accurate and high-quality measurements. First, after deploying the CTD system underwater, temperature measurements are taken before proceeding with data collection, and the descent rate is carefully controlled to not exceed 1 m/s. During data selection, we specifically focus on the descent phase of the CTD, as this segment is considered to be the least affected by external disturbances. This ensures that the selected data, including temperature, salinity, and pressure, are as accurate and undisturbed as possible. The raw.hex files are then converted into a manageable format through Data Conversion, extracting key parameters such as pressure, temperature, salinity, and density. A low-pass filter is applied to remove high-frequency noise, and bidirectional filtering is used to correct time offsets. Sensor calibration is performed using Align CTD to synchronize pressure, temperature, and conductivity measurements. Thermal effects on conductivity are corrected with the Cell Thermal Mass filter. Ship motion–induced fluctuations are addressed with Loop Edit, and derived oceanographic parameters, including depth, density, salinity, and sound velocity, are calculated. Finally, Bin Average is applied to average the data across specified depth intervals.

2.2 Sound speed calculation

The sound speed in seawater varies with salinity, temperature, and pressure, and empirical equations are typically used to express these relationships. These equations have been validated through extensive measurement data of sound speed in the sea, confirming their accuracy and applicability in practical scenarios. The Chen–Millero empirical equations (Wong and Zhu, 1995; Chen and

10.3389/fmars.2025.1489202

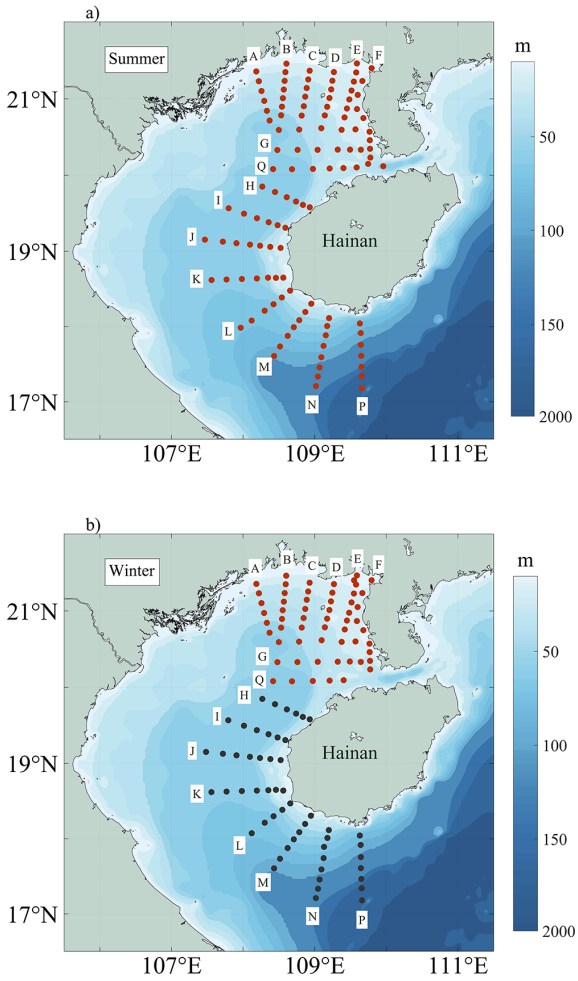

FIGURE 1
Topography (color codes) of the Beibu Gulf and Observation stations: **(A)** from 22 July to 10 August 2023 (red dots) and **(B)** from 9 to 18 December 2023 (red dots) and from 11 to 16 January 2024 (black dots).

Millero, 1977), which correlates sound speed with the thermohaline properties of water, is utilized for calculating sound speed at various depth and hydrographic stations using CTD data. The formula is expressed as follows:

$$c(S,T,P) = C_w(T,P) + A(T,P) + B(T,P)S^{\frac{3}{2}} + D(P)S^2 \quad (1)$$

where T = temperature (°C), S = salinity (‰, parts per thousand), and P = pressure (bar). $c(S,T,P)$ denotes the sound speed at various pressures. $C_w(T,P)$, $A(T,P)$ and $B(T,P)$ represents the correlation term involving temperature and pressure, and $D(P)$ represents the correlation term involving pressure. The formula is applicable within the range: 0°C < temperature < 40°C, 0‰ < salinity < 40‰, 0 bar < pressure < 1000 bar.

2.3 Sonocline calculation

Sonocline is the transition layer of sound speed, offering insight into the vertical structure of sound speed. The vertical gradient method is employed to calculate the sonocline in this paper. According to the Specifications for Oceanographic Survey (Li et al., 2011), in deep-sea conditions (water depth > 200 m), the absolute value of the mean sound speed gradient within the sonocline should approach 0.2 s^{-1}; whereas, in shallow water (water depth < 200 m), it should approach 0.5 s^{-1}. Additionally, the sound speed difference between the top and bottom layers of the sonocline should be not less than 1.0 m/s. The intensity of the sonocline is defined by the mean sound speed gradient within it. The thickness of the sonocline is defined as the vertical difference between its upper and lower boundaries. The depth of the sonocline is defined as the mean depth of these upper and lower boundaries. If multiple sonoclines are present in a sound speed profile, then the values described above are calculated on the basis of the first encountered sonocline, beginning from the sea surface. When sound speed increases with water depth, it is termed a positive sonocline; conversely, when it decreases, it is termed a negative sonocline. Based on the specific conditions observed in the Beibu Gulf, it has been established that the minimum threshold for the sound speed gradient within the sonocline is 0.40 s^{-1}.

2.4 Bellhop3D beam tracing model

A complete simulation of underwater sound propagation requires sound speed profiles, bathymetry, basic setting parameters, and a suitable underwater acoustic model. Underwater acoustic models are typically categorized into three main groups on the basis of governing equations and numerical methods: normal mode models (Porter, 1992; DeCourcy and Duda, 2020), parabolic equation models (Lin and Duda, 2012; Heaney and Campbell, 2016), and ray and beam tracing models (Porter, 2011; de Moraes Calazan and Rodríguez, 2018). The Bellhop3D beam tracing model (Porter, 2019), which falls into the third category, is employed to simulate sound propagation in the study area. Specifically designed for predicting acoustic pressure fields in 3D ocean environments, it is widely valued for its high precision.

Despite the trade-off of longer computation times due to its high accuracy, the Bellhop model is particularly suitable for this academic research, as we have sufficient time to run and tweak the model to ensure precision. This makes it appropriate for our study, where we prioritize detailed and clear physical descriptions of the acoustic field. This model builds upon the well-known Bellhop model by extending its capabilities into 3D environments and optionally incorporating horizontal refraction in the plane. It also allows users to calculate acoustic pressure fields using a 2D approach known as the Nx2D or 2.5D method along an array of radial lines (bearing lines) originating from the source. However, this approach does not account for sound energy refraction occurring outside the vertical plane of each bearing line.

The sound speed profile data used in this paper were derived from CTD data (see Sections 2.1 and 2.2). The bathymetric data utilized are sourced from the National Geophysical Data Center's 2–arc minute global relief data, ETOPO2 (https://www.ncei.noaa.gov/products/etopo-global-relief-model).

Below is a concise overview of the ray acoustics that underpin Bellhop 3D mode. The theory of ray acoustics (Jensen et al., 2011) interprets sound propagation as the radiation of numerous rays originating from a sound source, proposing that these rays follow Snell's law within the layered medium model. The following are two fundamental equations in ray acoustics, in the Cartesian coordinate system: the Eikonal equation and the intensity equation, presented as follows:

$$(\nabla\phi)^2 = \left(\frac{c_0}{c}\right)^2 = n^2(x, y, z) \tag{2}$$

$$\nabla \cdot (A^2 \nabla\phi) = 0 \tag{3}$$

here, $\nabla\phi$ denotes the ray direction, $c = c(x, y, z)$ represents the sound speed, c_0 is the reference sound speed, $n(x, y, z)$ stands for the refractive index, and $A = A(x, y, z)$ denotes the sound pressure amplitude. By solving the aforementioned equation, the ray trajectory and sound pressure amplitude can be determined.

The seabed properties were defined as follows: bottom density of 1.596 g/cm^3, bottom P-wave sound speed of 1579 m/s, and bottom P-wave absorption coefficient of 1 dB/λ (Liu and Lu, 2008). Sound propagation was simulated using Bellhop3D, with the 3D module selected for its ability to handle both vertical and horizontal coupling, making it ideal for large vessels and oil and gas exploration activities at 100 Hz, where emitted sounds are omnidirectional. For simulating sound propagation from marine organisms, the Nx2D module was used, as it effectively models vertical sound propagation without horizontal coupling, typical of marine organisms' vocalizations at this frequency. The source depth was set at 8 m with a vertical emission angle ranging from −5° to 15°. These seabed parameters were based on previous acoustic environment studies (Hamilton, 1980). Section 4.1 employs the Nx2D module for modeling biological sound propagation, whereas Section 4.2 utilizes the 3D module to simulate the propagation from anthropogenic sources. This approach ensures accurate simulations for both anthropogenic and biological sound propagation.

3 Seasonal sound speed variations

3.1 Seasonal variations of thermohaline properties

In the ocean, sound speed varies with temperature, salinity, and pressure. Therefore, understanding the fundamental properties of temperature and salinity is essential before analyzing the sound-speed field in a given region. The observational data reveal significant seasonal variations in temperature and salinity within the Beibu Gulf during the 2023–2024 observation period (Figures 2, 3).

3.1.1 Summer thermohaline structure

During the summer observation period (Figure 1A), sea surface temperature (at 3-m water depth) north of 20°N exceeds 29°C, gradually decreasing from nearshore area to offshore area, characterized by a north–south temperature gradient (Figure 2A). South of 20°N, temperature notably decreases, with central temperature dropping below 27°C. Minimal temperature differences are between the 20 m layer and the surface layer (Figure 2A). Below the 30 m, cold water expands northward, with increasing temperature differentials from surrounding areas. At 18° N, temperature drops to 22°C, which is 8°C lower than those north of 19°N. The cold water mass, positions between 17°N and 19.5°N, shifts approximately 1° southward compared to previous observations (Li et al., 2022), causing the 27°C isotherm to rise up to the sea surface at its core. Salinity within the cold water mass exceeds 32, contrasting notably with lower coastal salinity (Figure 2B). Sea surface salinity is consistently below 33 across the study area, exhibiting a north–south gradient. The nearshore low-salinity water extends outward from the northern Beibu Gulf coast north of 20.5°N at a shallow depth of 20 m. The mixing water with salinity of 32–33.5 is found below 30-m depth, as well as in the region between 19.5°N and 20.5°N. Vertically, mixing at 19.5°N–20.5°N shows uniformity, with minor temperature and salinity differences between surface and bottom layers. In summary, during summer, the northern Beibu Gulf is subject to freshwater influence, resulting in nearshore water densities below 1019 kg m^{-3},

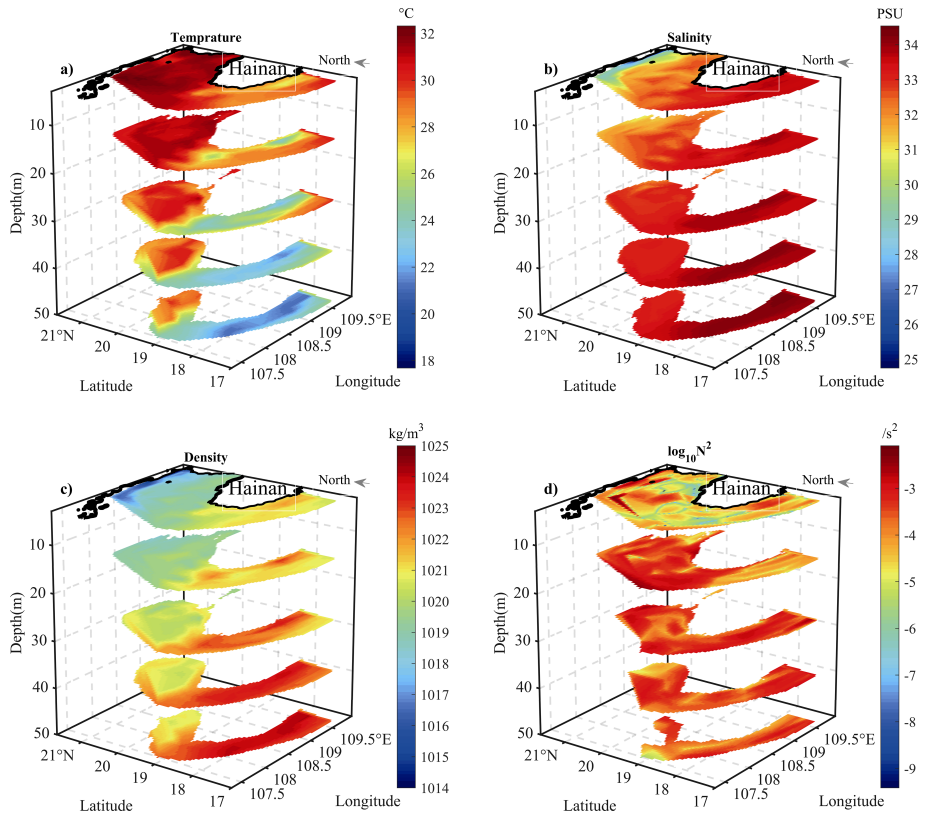

FIGURE 2
Distributions of water **(A)** temperature, **(B)** salinity, **(C)** density, and **(D)** buoyancy frequency on layers at different depths during summer observation in 2023. The geographical north is the ten o'clock direction of the figure.

whereas the southern part is impacted by cold, high-salinity water with densities ranging between 1,021 kg m^{-3} and 1,025 kg m^{-3} (Figure 2C). The majority of the buoyancy frequencies in the study area range from 10^{-4} s^{-2} to 10^{-3} s^{-2} (Figure 2D), indicating a strong stratification.

3.1.2 Winter thermohaline structure

Winter observations were conducted in two cruises separated by one month (Figure 1B). Horizontal distributions of temperature, salinity, and density across the observation area are shown in Figure 3. The seawater is vertically strong-mixed, with minor differences in temperature, salinity, and density between surface and deep layers. Temperature and salinity distributions in each layer exhibits similar patterns to historical data (Li et al., 2022): temperature increases from northeast coastal to southwest deep-water areas, with the coastal water below 23.5°C (Figure 3A). A warm tongue with temperature exceeding 25°C extends westward from the western side of Hainan Island to depths of up to 50 m (Figure 4A). Salinity ranges from 29 to 34.5, also increasing from northeast coastal to southwest areas, with coastal salinity below 30 and salinity exceeding 33 in the warm tongue area west of Hainan Island (Figure 4B). In winter, water density in the gulf primarily ranges from 1,020 kg m^{-3} to 1,023 kg m^{-3}. In the northern nearshore waters, it is characterized by lower temperature and salinity, with density between 21.5 kg m^{-3} and 22.5 kg m^{-3}. The gulf exhibits generally low buoyancy frequencies, indicative of weak stratification, with minimum values below 10^{-7} s^{-2}. In the northern part of the gulf, buoyancy frequencies are higher, reaching up to 10^{-4} s^{-2}.

3.1.3 Water mass analysis

Previous studies have indicated that the water masses in the Beibu Gulf primarily consist of the coastal water, mixed water, and open-ocean water, with a seasonal cold mass occurring during spring and summer (Chen et al., 2015). The sea temperature in the study area varied significantly seasonally; thus, the salinity that changed comparatively minor was often used as a criterion for water mass classification (Chen et al., 2011). This study primarily divides the water masses in the Beibu Gulf based on salinity: the coastal water is defined as having salinity below 32, the open-ocean water above 34, and the mixed water between 32 and 34. The properties of water masses in summer and winter are shown in Figure 4. The coastal water (north of 20.5°N) is depicted in blue and light blue, stations west of the Qiongzhou Strait in red, stations at 19°N–20°N in green and gray, and stations south of 19°N in black and purple. In summer, the northeast part of the Beibu Gulf is mainly composed of the coastal and mixed water, with the cold open-ocean water (low temperature and high salinity) located below 30-m depth in the southern part of the gulf. Shallow coastal stations (depth < 30 m) north of 20.5°N, characterized by low salinity, generally exhibit temperatures above 30°C. The cold mass

10.3389/fmars.2025.1489202

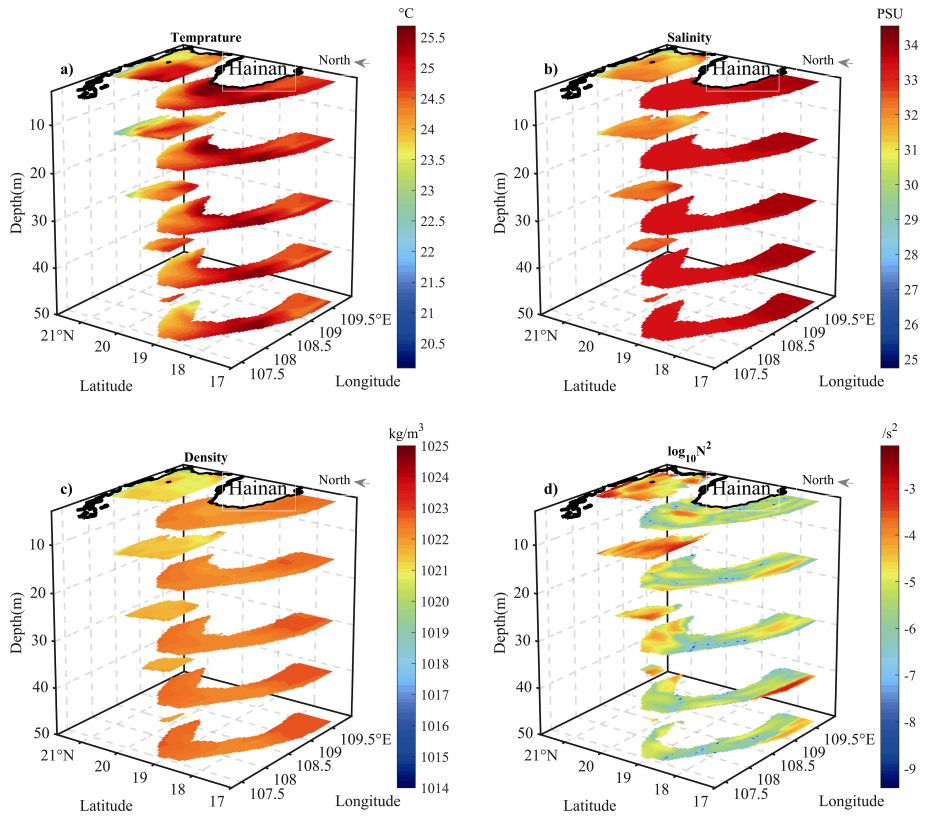

FIGURE 3
Distributions of water **(A)** temperature, **(B)** salinity, **(C)** density, and **(D)** buoyancy frequency on layers at different depths during winter observation in 2023 and 2024. The geographical north is the ten o'clock direction of the figure.

dominated by the open-ocean water (black and purple dots) with higher salinity up to 34.5 is found in the southern part of the gulf. Other stations mainly consist of the mixed water with salinity ranging from 32 to 33.5. In winter, the mixed water prevails; due to reduced runoff and precipitation (Liu et al., 2020), the extent of low-salinity coastal water contracts, with temperature dropping below 24°C. The open-ocean water with salinity exceeding 34 is only present below 100-m depth in the southern part of the gulf (Figure 4B).

Based on observations of temperature and salinity in summer and winter, two main sources contribute to water masses in the eastern Beibu Gulf: local coastal runoff and the northwest South China Sea shelf water entering through the southern gulf mouth. The seasonal temperature variations of these two water masses are evident, with the coastal water having higher temperature in summer and significantly lower temperature in winter, whereas the open-ocean water entering through the southern gulf mouth exhibits the opposite trend. Reduced runoff and precipitation in winter lead to a slight increase in salinity of the coastal water accordingly.

3.2 Seasonal thermohaline effects on sound speed

The observed data indicate significant seasonal variations in the thermohaline properties of the Beibu Gulf, affecting the sound speed profiles accordingly. During the summer of 2023 observation period, in the study area north of 19°N, the surface (3-m depth layer) sound speed generally exceeds 1,545 m/s. Influenced by coastal low-salinity water, sound speed increases outward from the northern coastal areas of the gulf. South of 19°N, the intrusion of cold open sea water significantly reduces sound speed, with minimum values dropping below 1,540 m/s in the surface layer. Vertically, north of 19°N, where temperature differences between the bottom and surface layers are minimal, sound speed primarily increases with pressure, with bottom-layer sound speed slightly greater than surface-layer sound speed (Figures 5A, B). South of 19°N, influenced by the cold water mass, deep-layer sound speed is notably lower than surface-layer sound speed, reaching a minimum (~1,532 m/s) at depths of 60–80 m. In summary, during the summer, the northern Gulf exhibits a north-high–south-low sound speed distribution pattern. In the northern gulf, deep-layer sound speed is slightly higher than surface-layer sound speed, whereas, in the southern gulf, deep-layer sound speed is significantly lower than surface-layer sound speed due to the influence of cold water mass.

During the winter observation period, due to decreased sea temperature compared to summer, sound speed also notably decreases. In the northeastern part of the Beibu Gulf (north of 20°N), the surface (3-m-depth layer) sound speed increases southwestward from the northern and eastern coastal areas (Figure 5C). In areas shallower than the 30-m isobath, sound speed is lower (~1,528 m/s), with minimal horizontal variability,

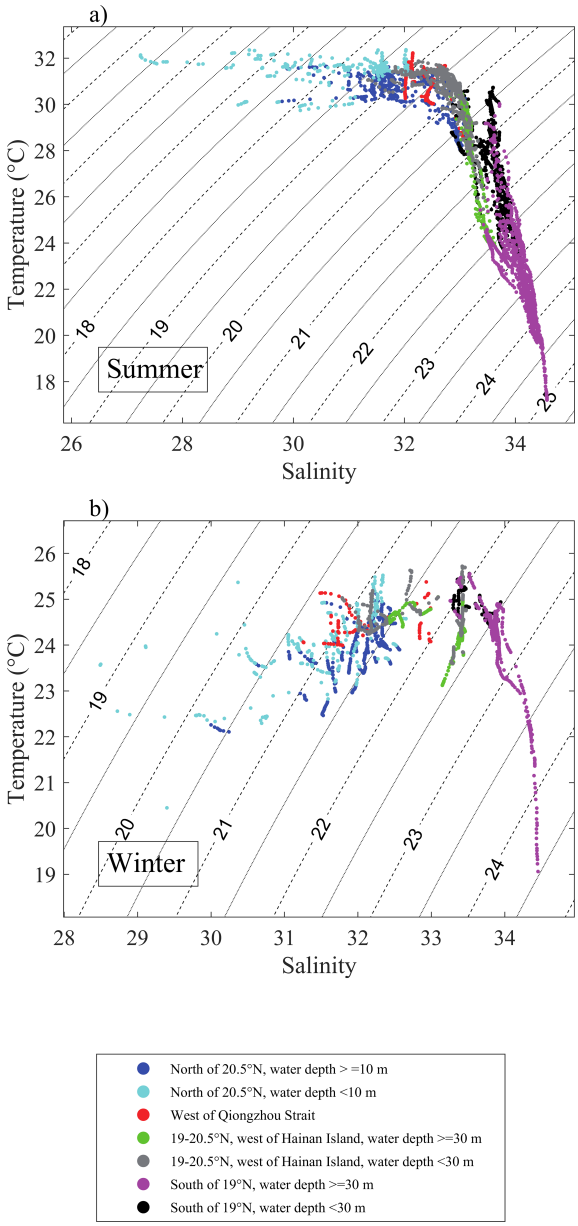

FIGURE 4
Temperature-Salinity (T-S) diagrams for observation in **(A)** summer and **(B)** winter (the dotted lines show the potential density).

whereas deeper areas beyond 30 m exhibit significant horizontal variability, with sound speed reaching up to 1,533 m/s. South of 20° N, surface sound speed distribution generally exhibits a north-low–south-high structure. On the west side of Hainan Island, within the shallow (<30 m) and southwest study area, two areas of peak sound speed are observed, exceeding surrounding speed by more than 1 m/s. Vertically, due to strong winter mixing, minimal temperature differences across the study area result in sound speed primarily increasing with pressure, reaching 1,550 m/s at 120-m depth (Figure 5D). Overall, the winter sound speed distribution in the northern Gulf shows a north-low–south-high structure. Notably, there are significant differences between the sound speed at shallower (<30 m) and deeper (≥30 m) stations and the horizontal sound speed gradients.

To further explore the underwater acoustic environment of the study area, we calculated the depth, thickness, and intensity of the sonocline using the vertical gradient method (Section 2.3) and classified them accordingly. Figure 6 shows the depths of different types of sonoclines in a) summer and b) winter, whereas Figure 7 presents the thicknesses, intensities, and typical sound speed profiles within the study region in a) summer and b) winter. In summer, influenced by the cold water mass, areas deeper than 30 m in the eastern Beibu Gulf predominantly exhibit negative sonoclines at depths ranging from 20 to 50 m, with strong intensities reaching up to 1.5 s^{-1}. In areas shallower than 30 m, influenced by coastal low-salinity water, sonoclines are predominantly positive or nonexistent, with weaker intensities generally not exceeding 0.8 s^{-1} compared to deeper areas. The thickness of these sonoclines is also smaller than

10.3389/fmars.2025.1489202

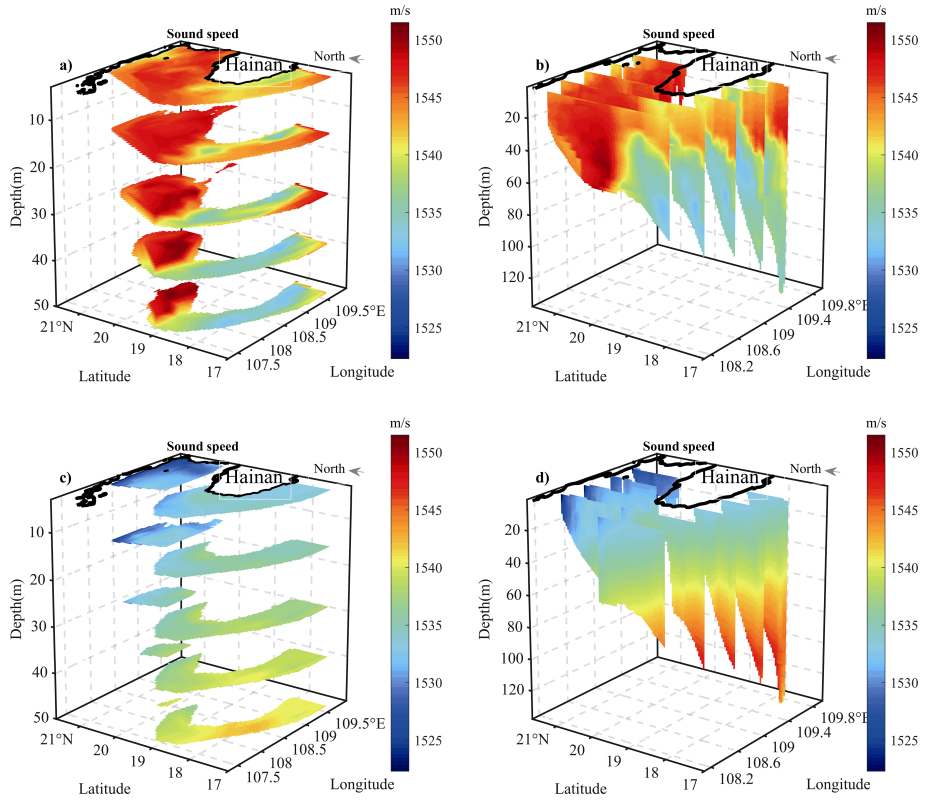

FIGURE 5
Seasonal variations in sound speed distributions on layers at different depths, **(A)** summer and **(C)** winter, and along the Meridian, **(B)** summer and **(D)** winter, in 2023–2024. The geographical north is the 10 o'clock direction of the figure.

those found in areas deeper than 30 m. During winter, due to strong mixing effects, the sound speed profiles throughout the eastern Beibu Gulf uniformly display negative gradient distributions. Sonoclines are only observed near the northwestern side of Hainan Island and a few coastal stations, whereas they are absent at other stations.

The sound-speed field in the Beibu Gulf exhibits distinctly different characteristics on either side of the 30-m isobath during both summer and winter. In summer, the horizontal distribution of the sound-speed field shows a north-to-south gradient, with a higher sound speed in the north and lower in the south. In regions where water depth is less than 30 m, sonoclines are predominantly positive or absent, with weak intensities (~0.8 s^{-1}) and small thicknesses. Conversely, in areas deeper than 30 meters, sonoclines predominantly exhibit negative gradients with

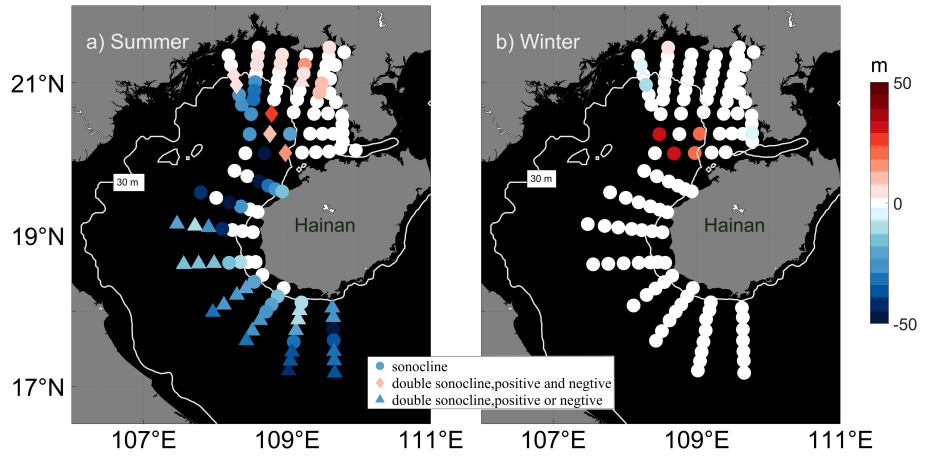

FIGURE 6
The depth of the sonocline (color) in **(A)** summer and **(B)** winter is represented as follows: red indicates a positive sonocline, whereas blue indicates a negative sonocline. Circular points denote stations where only one sonocline exists; a value of 0 signifies the absence of sonoclines. Diamond points indicate stations where both positive and negative sonoclines coexist, whereas triangular points indicate the presence of multiple positive or negative sonoclines. Additionally, the white line represents the 30-m isobath.

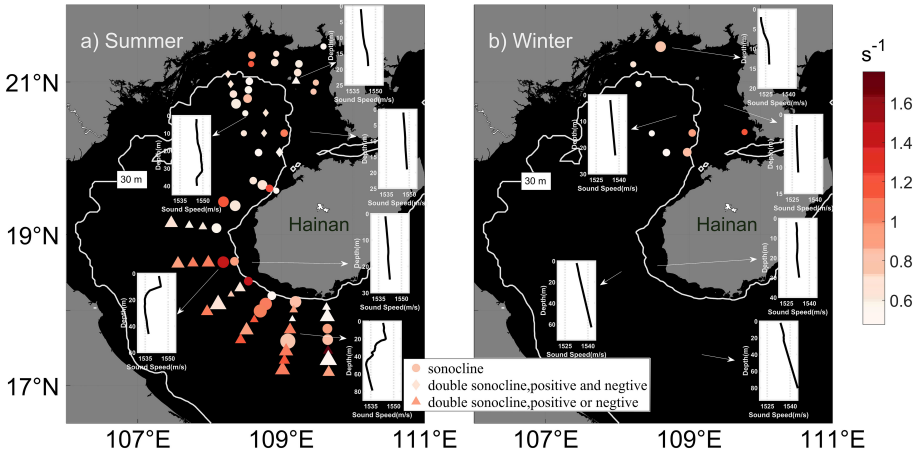

FIGURE 7
The thickness (size) and intensity (color) of the sonocline in **(A)** summer and **(B)** winter is represented as follows: circular points denote stations where only one sonocline exists; a value of 0 signifies the absence of sonoclines. Diamond points indicate stations where both positive and negative sonoclines coexist, whereas triangular points indicate the presence of multiple positive or negative sonoclines. The sound speed profile indicated by the gray arrow represents a typical profile for stations in the vicinity.

stronger intensities (~1.4 s^{-1}) and greater thicknesses. During winter, the sound-speed field in the Beibu Gulf reverses its summer pattern, showing a south-to-north gradient. North of 20°N and in regions where water depth is less than 30 m, the sound speed is approximately 5 m/s lower compared to the areas on the opposite side of the 30-m isobath, with minimal horizontal gradients within these regions. South of 20°N, specifically on the western side of Hainan Island where water depth is less than 30 m, a distinct area of maximum sound speed is observed, with sound speed differing by more than 1 m/s compared to surrounding sea areas.

4 Seasonal sound propagation variation

4.1 5-kHz sound source frequency

The 5-kHz frequency is commonly used by many aquatic animals for vocalizations (Ladich, 2019; Wang et al., 2013) and is also associated with various high-frequency oceanic sounds (Klusek and Lisimenka, 2016). To investigate sound propagation characteristics at this frequency, we set the source frequency to 5 kHz, source depth to 8 m, and vertical emission angle to range from −5° to 15° (further details in Section 3.4).

Based on the significant differences of sound-speed field observed on either side of the 30-m isobath, as discussed in Section 3.2, we divided the study area into nearshore (water depth < 30 m) and offshore (water depth > 30 m) regions. Sound propagation was simulated at 12 stations (6 nearshore and 6 offshore) within these two areas (Figure 8). Although sediment parameters can vary with geographical location, in this study, they were set based on the predominant sediment types in the Beibu Gulf without accounting for variations.

Figures 9A–L, 10A–L depict the three-dimensional transmission loss at a 5-kHz sound source frequency during the summer and winter seasons in the study area, presenting data from a top view at a water depth of 10 m. To better illustrate the differences in sound transmission loss, we have highlighted the locations of 60-dB transmission loss with red lines in the figure. The distance at which the transmission loss reaches 60 dB from the source location is defined as the effective distance. These effective distances in all horizontal directions define the effective area. Figures 9M, 10M present the mean effective distance (bars) and effective area (dots) during summer and winter. In summer, when receiver depth (RD) = 10 m (Figure 9), the effective distance at nearshore stations with water depth less than 30 m (Figures 9A–F) extends beyond 15 km, whereas offshore stations (Figures 9G–L), with water depth exceeding 30 m, generally exhibit effective distances within 10 km. After averaging the effective distances in each direction (Figure 9M), it is observed that, during summer, the maximum mean effective distance at nearshore stations approaches 12 km, with a minimum of approximately 6 km, and the effective area ranges from 109 km^2 to a maximum of 413 km^2. In contrast, offshore stations show mean effective distances consistently below 6 km, with a maximum effective area of only 96 km^2.

This suggests that 5-kHz sounds travel longer distances and are more easily detected in nearshore areas with water depths less than 30 m. The variation in effective distances between nearshore and offshore areas is attributed to differences in their sound-speed fields. Sound rays tend to refract toward regions with lower sound speed; in nearshore areas, where the sonocline is primarily positive or absent and where sound speed increasing with depth, sound rays refract toward the sea surface and propagate in the surface sound channel, thereby enhancing propagation distance. In offshore areas, characterized by a negative sonocline, where sound speed decreases with depth, sound rays refract toward the seabed, resulting in frequent sound energy attenuation upon contact. In winter (Figure 10), effective distances in nearshore areas generally exceed

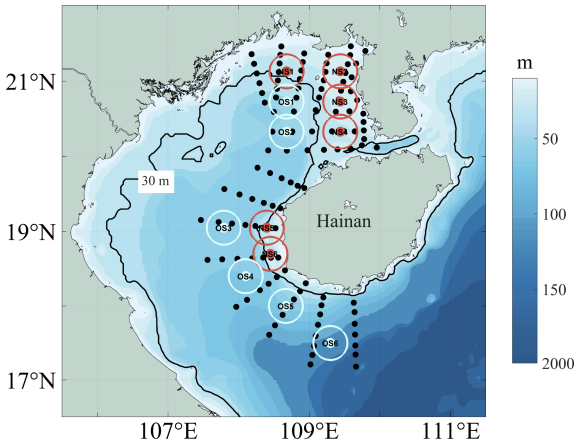

FIGURE 8
Topography (color codes) of the Beibu Gulf and Observation stations (black dots). Simulation of sound propagation: Positions of sound sources, with six red nearshore sound source stations located in areas with depths less than 30 m and with six white offshore sound source stations situated in areas with depths exceeding 30 m. Circles represent a radius of 25 km.

those in offshore areas, further supporting the conclusion that sounds are more effectively transmitted and received in nearshore area. However, compared to summer, the maximum mean effective distance in nearshore areas decreases by 3 km to 9 km, and the maximum effective area decreases by 188 km^2 to 288 km^2. In contrast, the mean effective distance and effective area in offshore areas remain relatively stable, with maximum values of approximately 6 km and 96 km^2, respectively. The seasonal variation is attributed to vertically uniform mixing in the study area during winter, which results in minimal vertical gradients in sound speed and the absence of a surface sound channel conducive to sound propagation.

4.2 100-Hz sound source frequency

The primary frequency of noise generated by large vessels and oil and gas exploration activities is around 100 Hz (Johnston and Cain, 1982; Larayedh et al., 2024; Santos-Domínguez et al., 2016), with sound source levels exceeding 250 dB and broad directivity (Greene and Richardson, 1988), making them major contributors to low-frequency ocean noise. To investigate sound propagation at this frequency, we set the source depth to 8 m, frequency to 100 Hz, and vertical emission angle from −90° to 0° (further details in Section 3.4). Sound propagation was simulated at 12 stations (6 nearshore and 6 offshore) (Figure 10).

Figures 11A–L, 12A–L illustrate the three-dimensional transmission loss at a 100-Hz sound source frequency during the summer and winter seasons in the study area, presenting data visualized from a top view at a water depth of 10 m. Consistent with Section 4.1, locations of 60-dB transmission loss are highlighted in Figures 11, 12. Figures 11M, 12M present the mean effective distance (bars) and effective area (dots) for summer and winter. In summer, at a receiving depth of 10 m, the mean effective distance ranges from over 5 km to more than 13 km, whereas the mean effective area varies between 98 km^2 and 608 km^2. In contrast, during winter, the mean effective distance does not exceed 6 km, and the mean effective area ranges from 19 km^2 to 114 km^2. The effective sound propagation distance and area in summer are significantly greater than in winter, aligning with the sound propagation characteristics observed at a 5-kHz source frequency in Section 4.1. However, at the 5-kHz frequency, both the mean effective distance and the mean effective area at nearshore stations exceeded those at offshore stations during both seasons. Conversely, at the 100-Hz frequency, this phenomenon is not observed. When comparing stations at the 100-Hz frequency, only nearshore stations 4–6 exhibit mean effective distances and areas greater than their offshore counterparts, with nearshore station 5 and station 6's mean effective areas being only 1 km^2 and 46 km^2 larger than those of offshore stations 5 and 6, respectively.

5 Discussion

5.1 Comparison with other regional studies

The current research delves into the sound-speed field and sound propagation traits in the Beibu Gulf, taking into account their seasonal changes. When juxtaposed with similar environments, such as other bays or shallow waters, Beibu Gulf stands out with distinct features. Notably, in the Arabian Gulf (Abdelrahman, 1998), known for its analogous water depths, the summer season is marked by a consistent negative sonocline spanning depths from 20 m to 40 m, leading to a sound speed variance of around 20 m/s from the surface to the seabed. Conversely, during the summer months in Beibu Gulf, the coastal region (with water depths less than 30 m) either exhibits positive sonoclines or lacks them entirely, maintaining a uniform sound speed from top to bottom. In deeper offshore waters (exceeding 30 m), positive sonoclines dominate with a surface-to-bottom sound speed difference approximating 20 m/s. In winter, the Arabian Gulf partially homogenizes vertically in sound speed, with a minor difference of about 4 m/s from surface to

10.3389/fmars.2025.1489202

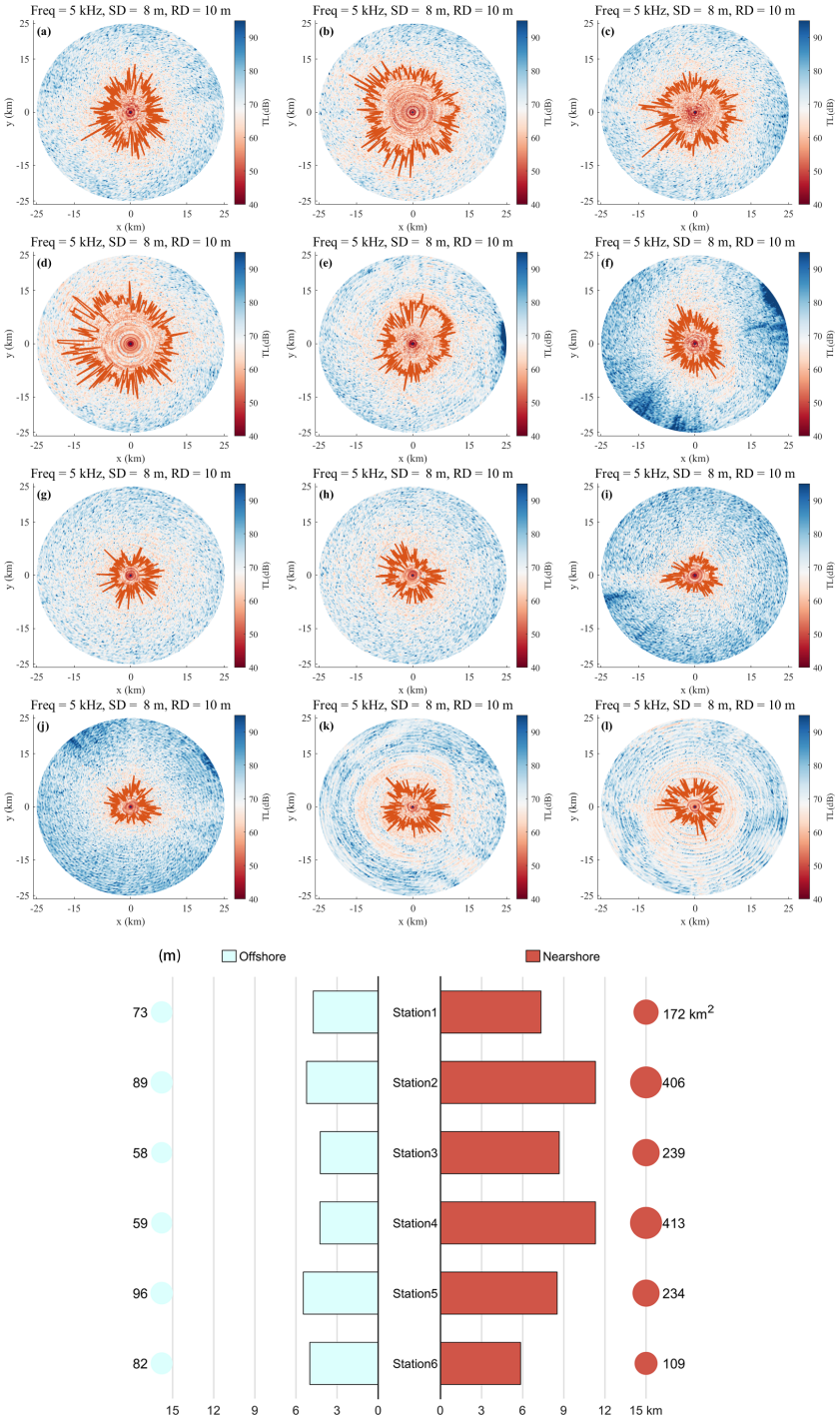

FIGURE 9
The three-dimensional distribution of transmission loss in the study area by Bellhop3D Nx2D, the top view, when the 5-kHz sound source is in the nearshore and offshore sound source stations. Red line represents the effective area. **(A–F)** Summer, nearshore, SD = 8 m, RD = 10 m. **(G–L)** Summer, offshore, SD = 8 m, RD = 10 m. **(M)** Mean effective distance (bars) and effective area (dots) in summer.

bottom. In stark contrast, the Beibu Gulf is characterized by a lack of sonoclines, where coastal differences are about 5 m/s, and offshore measures around 20 m/s.

The fundamental divergence in sound propagation between these regions stems largely from the variations in their sound speed fields. Specifically, the Beibu Gulf's nearshore areas benefit acoustically from positive sonoclines that enhance upper ocean layer sound transmission, whereas its offshore areas' negative sonoclines obstruct such propagation, a stark contrast to the Arabian Gulf's intermediate characteristics due to its lack of sonoclines. This core difference leads to pronounced sound propagation attributes unique to Beibu Gulf. Utilizing a 5-kHz source with a vertical emission angle ranging between −5° and 15°, it is evident that sound travels further distances nearshore compared to offshore, markedly so in summer.

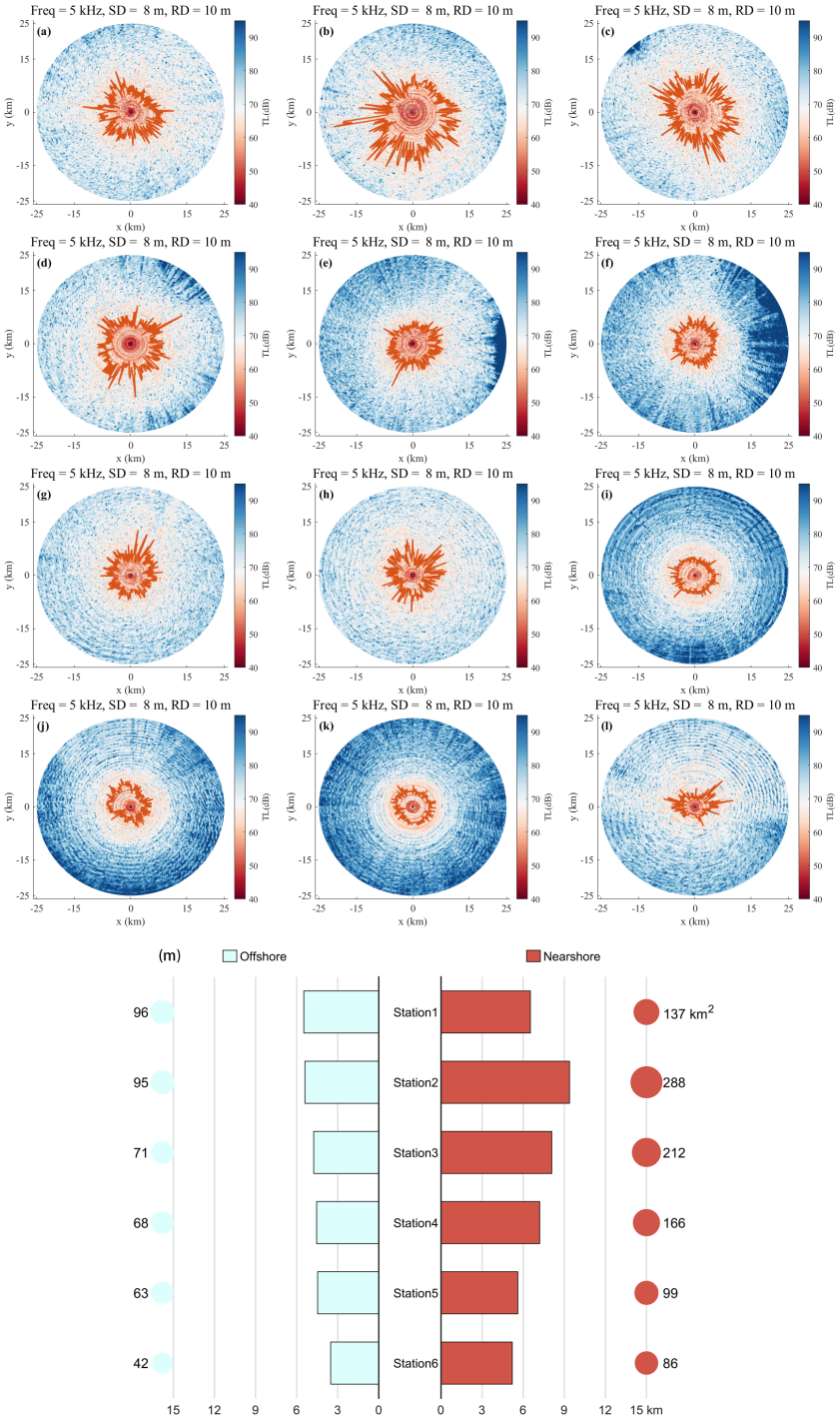

FIGURE 10
The three-dimensional distribution of transmission loss in the study area by Bellhop3D Nx2D, the top view, when the 5-kHz sound source is in the nearshore and offshore sound source stations. Red line represents the effective area. **(A–F)** Winter, nearshore, SD = 8 m, RD = 10 m. **(G–L)** Winter, offshore, SD = 8 m, RD = 10 m. **(M)** Mean effective distance (bars) and effective area (dots) in winter.

This pattern is absent in both the Arabian Gulf and Gulf Stream (Levenson and Doblar, 1976; Mellberg et al., 1990). In contrast, other shallow regions like those in the South China Sea demonstrate an opposite tendency (Liu et al., 2023), where offshore propagation distances surpass nearshore distances. This underscores the need for special consideration of the Beibu Gulf's sound-speed field and propagation characteristics.

5.2 Effect of sound speed horizontal gradient

In Section 4.1, it is noted that, in the sound propagation simulation, sounds propagate further in the nearshore area compared to the offshore area. This difference is primarily attributed to significant variations in sound field distribution

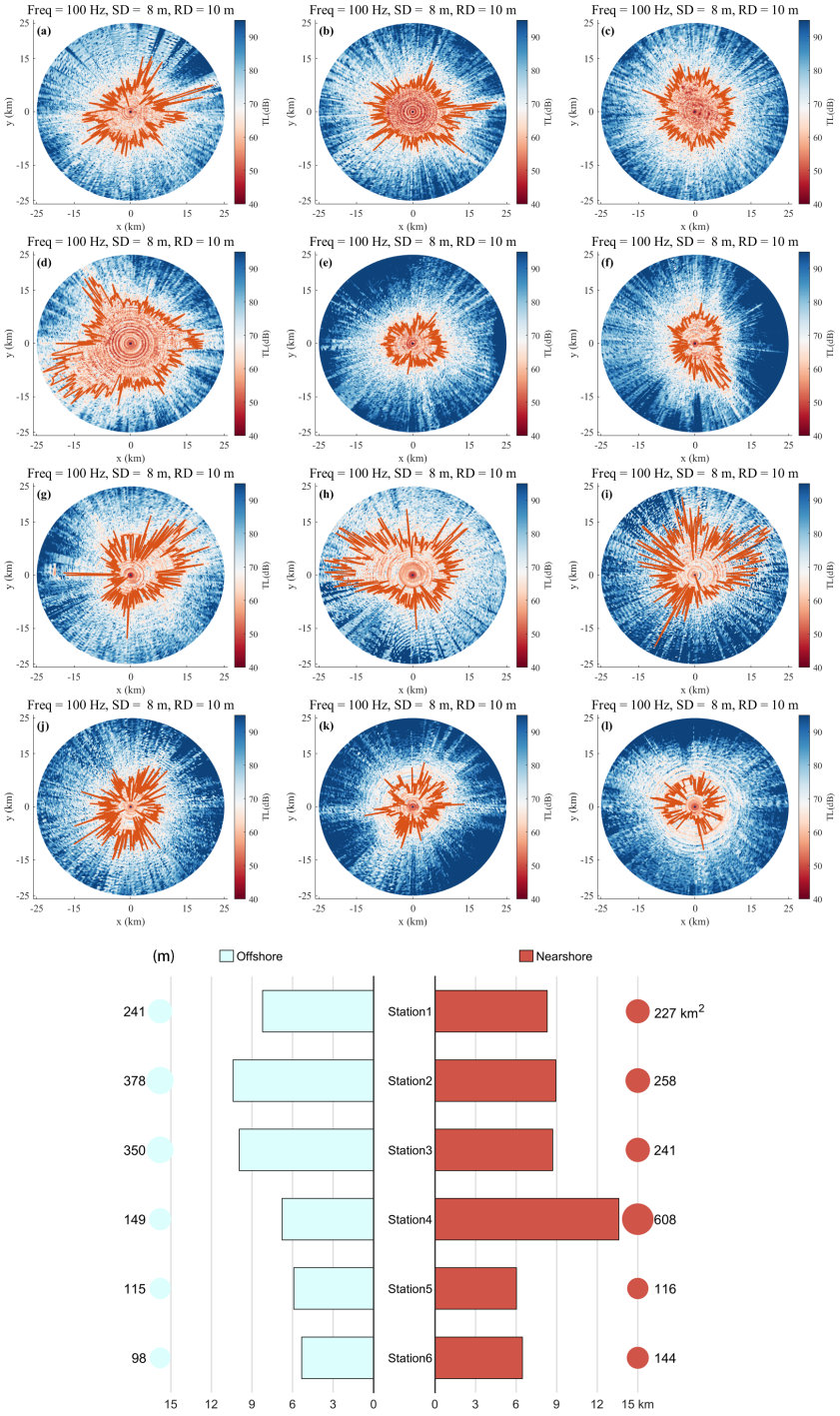

FIGURE 11
The three-dimensional distribution of transmission loss in the study area by Bellhop3D 3D, the top view, when the 100-Hz sound source is in the nearshore and offshore sound source stations. Red line represents the effective area. **(A–F)** Winter, nearshore, SD = 8 m, RD = 10 m. **(G–L)** Winter, offshore, SD = 8 m, RD = 10 m. **(M)** Mean effective distance (bars) and effective area (dots) in winter.

between these two zones. Sound propagation in seawater is influenced not only by sound-speed field distribution but also by environmental parameters such as topography and boundary characteristics, particularly pronounced in shallow waters where topography significantly affects sound transmission (Liu et al., 2023). To verify if the phenomenon observed in Section 4.1 is primarily due to sound-speed field distribution, sensitivity experiments were conducted. These experiments involved setting the entire study area's sound speed profile to a uniform profile, ensuring no horizontal variation in the sound field direction while keeping other parameters consistent with those used in the simulations in Section 4.1.

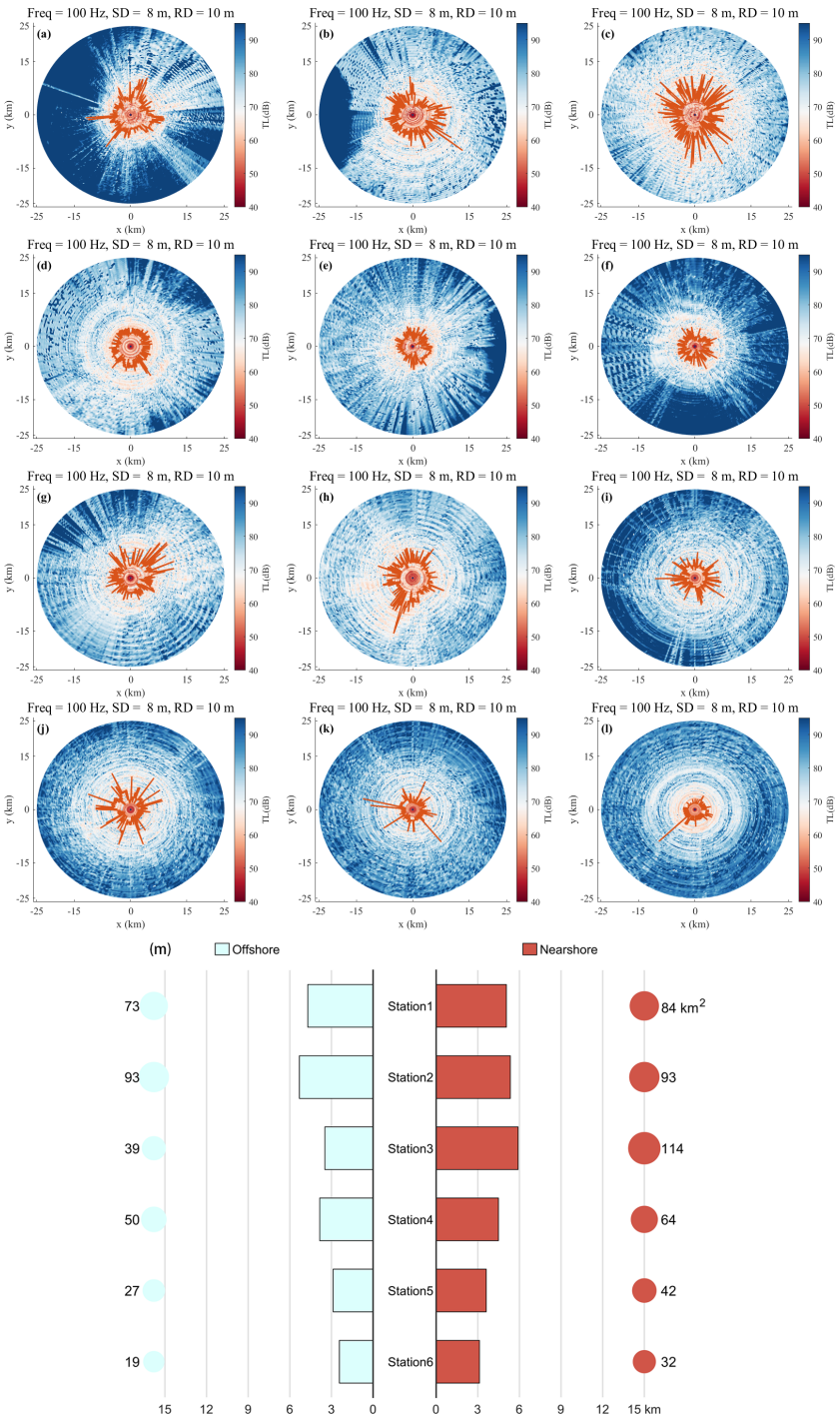

FIGURE 12
The three-dimensional distribution of transmission loss in the study area by Bellhop3D 3D, the top view, when the 100-Hz sound source is in the nearshore and offshore sound source stations. Red line represents the effective area. **(A–F)** Summer, nearshore, SD = 8 m, RD = 10 m. **(G–L)** Winter, offshore, SD = 8 m, RD = 10 m. **(M)** Mean effective distance (bars) and effective area (dots) in summer.

Figure 13 illustrates the simulated sound transmission loss, visualized in a uniform horizontal sound field. The distribution of transmission loss at nearshore stations (Figures 13A–F) and offshore stations (Figures 13G–L) appears similar, with minimal transmission loss within a 15-km radius and a peak at around 18 km. The effective distance is also similar, generally not exceeding 10 km. Compared to simulations under varying horizontal sound fields, significant reductions in the effective distance are observed at nearshore stations, with the maximum mean effective distance decreasing from approximately 12 km to 6 km, and the maximum effective area reducing from 413 km² to 147 km². Conversely, at offshore stations, there is a slight increase in the effective area, from less than

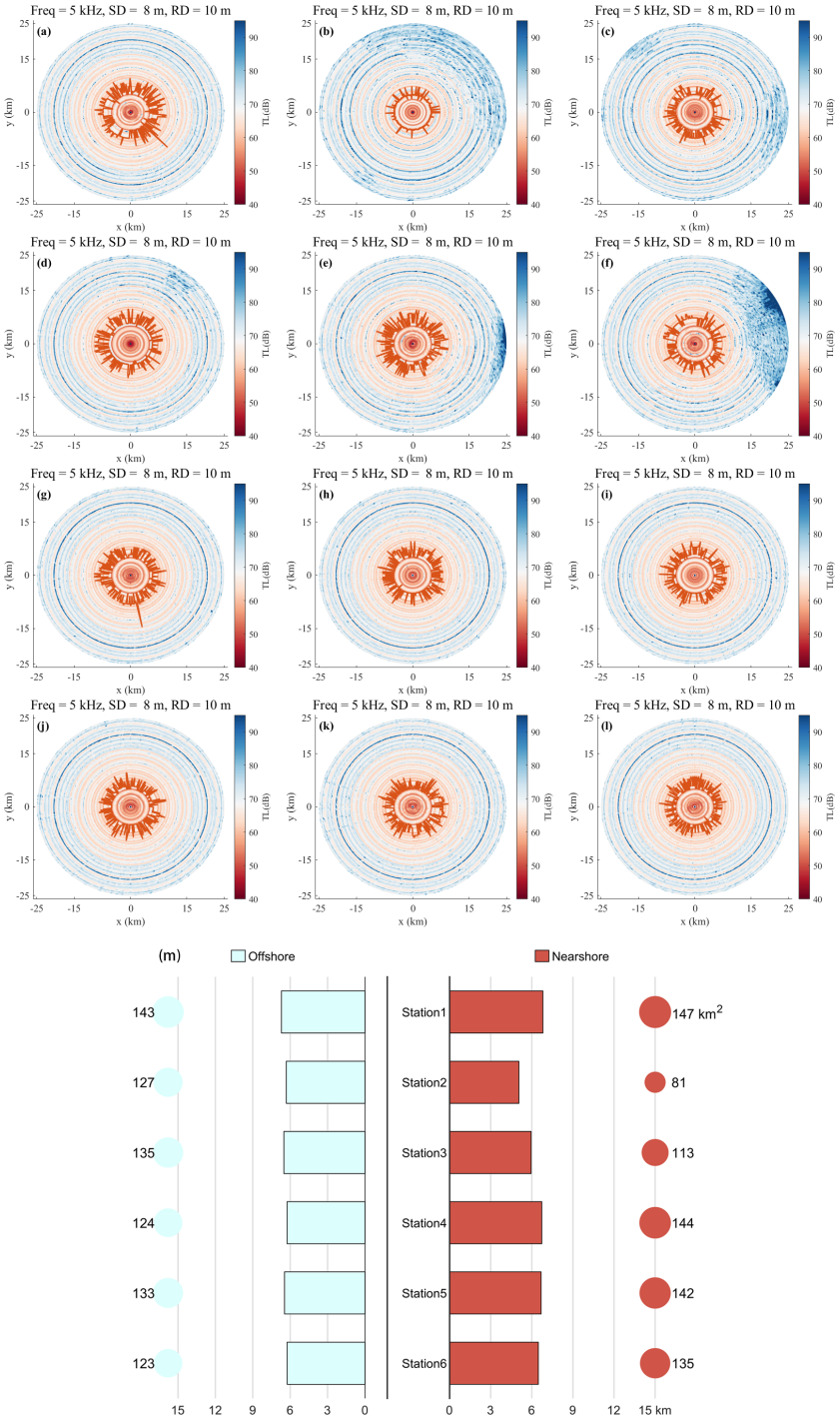

FIGURE 13
The three-dimensional distribution of transmission loss in the study area by Bellhop3D Nx2D, the top view, when the sound source is in the nearshore and offshore sound source stations. Red line represents the effective area. **(A–F)** Summer, nearshore, SD = 8 m, RD = 10 m. **(G–L)** Summer, offshore, SD = 8 m, RD = 10 m. All sound-speed profiles are consistent. **(M)** Mean effective distance (bars) and effective area (dots) in summer.

100 km² to a maximum of 143 km². Overall, the distribution of sound transmission loss at a water depth of 10 m under uniform horizontal simulation is very similar in both nearshore and offshore areas, indicating that sound-speed field distribution in the Beibu Gulf is a crucial factor in the sound propagation. The observation that sounds propagate further nearshore due to sound-speed field distribution is well-supported.

5.3 Physical mechanisms behind the seasonal variation of sound speed

The seasonal variation of sound speed in the Beibu Gulf is primarily driven by the collaboration of temperature, salinity, and water mass distribution, exhibiting significant spatiotemporal fluctuations. During the summer, a distinct cold water mass

forms between latitudes 17°N and 19.5°N, with water temperatures up to 8°C lower than the surrounding water at the same depth. The salinity in this cold water mass is also relatively high, increasing from north to south. It is widely stated that this cold water mass is the remnant of the South China Sea's cold water intrusion, which appears in the spring and dissipates in the autumn (Li et al., 2022; Chen et al., 2015). Our summer observations coincided with the peak formation period of this cold water mass. In the absence of other environmental changes, the temperature drop leads to a reduction in sound speed. Therefore, the sound speed within the cold water mass is lower than that of the surrounding water, forming a negative sonocline. This is consistent with observed phenomena: the sound speed inside the cold water mass is significantly lower, and a negative sonocline is commonly observed in the area where the cold water mass occurs. The sound speed in the north of Beibu Gulf are primarily influenced by the low-salinity nearshore water masses covering the upper layers, which results in lower sound speed in these surface waters.

During winter, the temperature distribution reverses, with the southern waters being warmer than those in the north. This is mainly due to the land temperature being lower than the ocean temperature during the winter months. The northern waters are more influenced by land and are mainly composed of nearshore water masses. As a result, the sound speed field reverses, with higher sound speed in the southern waters and lower sound speed in the northern waters. Furthermore, the strong winter winds enhance vertical mixing (Li et al., 2022), leading to a more uniform distribution of temperature and salinity. This vertical mixing effect causes the winter sonocline to dissipate, particularly in shallow water regions.

In summary, the primary physical mechanisms driving sound-speed field in the Beibu Gulf include the residual effect of the South China Sea's cold water intrusion, the influence of low-salinity nearshore waters, and the vertical mixing caused by winter winds.

5.4 Potential impacts on the Indo-Pacific humpback dolphins

In Section 4.1, we simulated the high-frequency sound propagation of marine organisms by setting the source frequency to 5 kHz, the source depth to 8 m, and the vertical emission angle ranging from −5° to 15°. The results indicated that sound propagation distances in nearshore areas (with water depths < 30 m) were significantly greater than those in offshore areas (with water depths > 30 m). This suggests that marine organisms (Hildebrand, 2009) in shallower waters have a greater ability to send and receive sounds.

This finding aligns with the habitat preferences of Indo-Pacific humpback dolphins, a protected species in the study area, which are found exclusively in waters less than 30 m deep (Li et al., 2016; Lin et al., 2022). Previous attempts to explain their preference for shallow waters have focused on food resources and hydrological conditions but have yielded inconclusive results (Yong et al., 2023). However, recent acoustic tagging and behavioral studies provide direct evidence of their responsiveness to environmental acoustics (Yong et al., 2023), indicating that quieter environments enhance their communication efficiency and social behaviors, offering a direct acoustic advantage.

Furthermore, the acoustic environment plays a pivotal role in the life of many marine species, with recent studies highlighting the importance of sound for communication, navigation, foraging, and predator avoidance across diverse marine organisms (Popper and Hawkins, 2019). Our expanded discussion includes behavioral observations that reveal the Indo-Pacific humpback dolphins' reliance on sound extends to complex social interactions and essential survival tasks. Such behaviors are facilitated by acoustic conditions in shallower waters, aligning with their observed habitat preferences. Additionally, various fish species demonstrate significant behavioral alterations in response to sound changes. Many fishes rely on acoustic cues for spawning and navigation, and noise pollution may mask these critical signals. The disruption of predator–prey dynamics due to anthropogenic noise further highlights the need for comprehensive conservation strategies.

The Indo-Pacific humpback dolphin has evolved to rely heavily on acoustics, with a specialized auditory system (Au and Hastings, 2008). These dolphins depend on an appropriate acoustic environment for survival, including sound for communication, territorial displays, food detection, mate selection, and predator avoidance. The Beibu Gulf's biodiversity supports over 700 Indo-Pacific humpback dolphins inhabiting waters less than 30 m deep (Yong et al., 2023). This acoustic advantage likely contributes to their preference for shallow waters, which is a key factor in their habitat selection.

Our study also highlights the significant influence of temperature and salinity on sound speed in the ocean, providing new insights into sound propagation dynamics. These findings offer potential implications for protecting the habitats and behaviors of species like the Indo-Pacific humpback dolphin. Given the context of global climate change, variations in temperature and salinity may have profound effects on the survival and reproduction of cetacean populations.

Investigating the implications of such variations on vital activities of marine mammals is critical, as a significant portion of marine life relies on sound. Therefore, we recommend that trends in temperature and salinity be considered when formulating marine conservation policies, particularly with regard to dynamic monitoring through acoustic technologies to protect key habitats. As climate change drives environmental variability, safeguarding the acoustic integrity of marine ecosystems is fundamental to preserving biodiversity and ecological functions.

6 Summary

In this study, we explored the seasonal variations of temperature and salinity in the Beibu Gulf and their impact on the sound-speed field. Using the Bellhop3D beam tracing model, we simulated sound propagation at 5-kHz and 100-Hz frequencies between nearshore and offshore areas and confirmed through sensitivity experiments

the critical influence of horizontal sound-speed field variations on sound propagation. Key findings are as follows:

1. In summer, a distinct north–south temperature gradient is observed, with a cold water mass appearing between 17°N and 19.5°N, showing temperatures up to 8°C lower than surrounding waters, and higher salinity over 32. In winter, temperature and salinity are higher in the south, with uniform vertical mixing, indicating complex water mass interactions.
2. The sound-speed field in summer shows higher values in the north, with positive or absent sonoclines in shallow areas and negative sonoclines in deeper regions. Winter reverses this pattern, impacting sound propagation paths significantly across the 30-m isobath.
3. At a 5-kHz frequency, summer conditions in nearshore regions (depth < 30 m) enhance sound propagation due to predominantly positive sonoclines, achieving greater effective distances and areas compared to offshore regions. This pattern persists in winter, although effective ranges decrease slightly due to strong mixing and reduced vertical gradient.
4. At a 100-Hz frequency, summer propagation demonstrates superior capacity, with mean effective distances up to 13 km, whereas winter conditions limit effective range to 6 km. The differences in propagation characteristics between frequencies highlight the seasonal and frequency-dependent nature of sound propagation.

This study investigates the distribution of sound speed and the characteristics of sound propagation in the Beibu Gulf during both summer and winter, examining the underlying physical mechanisms and potential impacts on Indo-Pacific humpback dolphins. Although the study provides valuable preliminary insights into sound propagation, several limitations remain.

First, our analysis is geographically and seasonally specific. Future research should aim to expand this scope by examining Indo-Pacific humpback dolphin habitats across various ecosystems globally, incorporating a more comprehensive range of seasonal variations to gain a broader understanding of acoustic environments worldwide.

Second, this study primarily focuses on the effects of temperature and salinity on sound speed, without addressing the potential influence of other environmental factors, such as ocean currents, pollution, and human activities. Future studies could integrate multidimensional environmental data and monitor the impact of anthropogenic noise pollution and other human activities on the acoustic environment. This approach would be enriched by employing advanced sensor technologies, remote sensing methods, and data analytics to further investigate how these factors influence marine mammal behavior and ecosystem dynamics.

Additionally, examining the interplay between natural and anthropogenic factors and their combined effect on sound propagation could provide deeper insights into the mitigation measures necessary to protect marine life. Continuous development of predictive models that incorporate these diverse elements could significantly enhance conservation strategies for marine ecosystems.

Data availability statement

The raw data supporting the conclusions of this article will be made available by the authors, without undue reservation.

Ethics statement

The manuscript presents research on animals that do not require ethical approval for their study.

Author contributions

FZ: Writing – original draft, Writing – review & editing. LX: Conceptualization, Investigation, Supervision, Writing – review & editing. ML: Data curation, Investigation, Writing – review & editing. QL: Data curation, Investigation, Writing – review & editing. SL: Formal analysis, Funding acquisition, Writing – review & editing.

Funding

The author(s) declare financial support was received for the research, authorship, and/or publication of this article. This study was supported by National Nature Science Foundation of China (42276019), Guangdong Provincial Observation and Research Station for Tropical Ocean Environment in Western Coastal Waters (GSTOEW; 2024B1212040008), the lnnovation Team Plan for Universities in Guangdong Province (2019KCXTF021 and 2023KCXTD015), Guangdong Provincial "Chasing Excellence" Special Fund (231419012, 231919030), and NSFC Shiptime Sharing Project: NORC2023-11 2023 Beibu Gulf Scientific Expedition and Experimental Research (42249911).

Conflict of interest

The authors declare that the research was conducted in the absence of any commercial or financial relationships that could be construed as a potential conflict of interest.

Publisher's note

References

Abdelrahman, S. M. (1998). Seasonal variations of sound speed in the Arabian Gulf. *Oceanologica Acta* 21, 59–68. doi: 10.1016/S0399-1784(98)80049-2

Affatati, A., Scaini, C., and Salon, S. (2022). Ocean sound propagation in a changing climate: Global sound speed changes and identification of acoustic hotspots. *Earth's Future* 10, e2021EF002099. doi: 10.1029/2021EF002099

Au, W. W., and Hastings, M. C. (2008). *Principles of marine bioacoustics* Vol. 510 (New York: Springer). doi: 10.1007/978-0-387-78365-9

Chen, C. T., and Millero, F. J. (1977). Speed of sound in seawater at high pressures. *J. Acoustical Soc. America* 62, 1129–1135. doi: 10.1121/1.381646

Chen, S., Li, Y., Hu, J., Zheng, A., Huang, L., and Lin, Y. (2011). Multiparameter cluster analysis of seasonal variation of water masses in the eastern Beibu Gulf. *J. oceanography* 67, 709–718. doi: 10.1007/s10872-011-0071-y

Chen, Z., Qiao, F., Xia, C., and Wang, G. (2015). The numerical investigation of seasonal variation of the cold water mass in the Beibu Gulf and its mechanisms. *Acta Oceanologica Sin.* 34, 44–54. doi: 10.1007/s13131-015-0595-x

DeCourcy, B. J., and Duda, T. F. (2020). A coupled mode model for omnidirectional three-dimensional underwater sound propagation. *J. Acoustical Soc. America* 148, 51–62. doi: 10.1121/10.0001517

de Moraes Calazan, R., and Rodríguez, O. C. (2018). Simplex based three-dimensional eigenray search for underwater predictions. *J. Acoustical Soc. America* 143, 2059–2065. doi: 10.1121/1.5030922

Ermolaev, V., and Bui, T. G. (2014). "Modeling of noise and acoustic field calculations in the limited water area of Beibu gulf using geospatial data," in *Information Fusion and Geographic Information Systems (IF AND GIS 2013) Environmental and Urban Challenges*, Luxembourg: Springer 277–287. doi: 10.1007/978-3-642-31833-7_18

Gao, J., Wu, G., and Ya, H. (2017). Review of the circulation in the beibu gulf, South China Sea. *Continental Shelf Res.* 138, 106–119. doi: 10.1016/j.csr.2017.02.009

Greene, J. C.R., and Richardson, W. J. (1988). Characteristics of marine seismic survey sounds in the Beaufort Sea. *J. Acoustical Soc. America* 83, 2246–2254. doi: 10.1121/1.396354

Hamilton, E. L. (1980). Geoacoustic modeling of the sea floor. *J. Acoustical Soc. America* 68, 1313–1340. doi: 10.1121/1.385100

Heaney, K. D., and Campbell, R. L. (2016). Three-dimensional parabolic equation modeling of mesoscale eddy deflection. *J. Acoustical Soc. America* 139, 918–926. doi: 10.1121/1.4942112

Hildebrand, J. A. (2009). Anthropogenic and natural sources of ambient noise in the ocean. *Mar. Ecol. Prog. Ser.* 395, 5–20. doi: 10.3354/meps08353

Jensen, F. B., Kuperman, W. A., Porter, M. B., Schmidt, H., and Tolstoy, A. (2011). *Computational ocean acoustics* Vol. 2011 (New York, NY: Springer New York). doi: 10.1007/978-1-4419-8678-8

Johnston, R. C., and Cain, B. C. (1982). "Marine seismic energy sources: acoustic performance comparison," in *Offshore Technology Conference (OTC)*, USA: AIP (American Institute of Physics) OTC–4255. doi: 10.4043/4255-MS

Klusek, Z., and Lisimenka, A. (2016). Seasonal and diel variability of the underwater noise in the Baltic Sea. *J. Acoustical Soc. America* 139, 1537–1547. doi: 10.1121/1.4944875

Koongolla, J. B., Lin, L., Pan, Y. F., Yang, C. P., Sun, D. R., Liu, S., et al. (2020). Occurrence of microplastics in gastrointestinal tracts and gills of fish from Beibu Gulf, South China Sea. *Environ. Pollut.* 258, 113734. doi: 10.1016/j.envpol.2019.113734

Ladich, F. (2019). Ecology of sound communication in fishes. *Fish fisheries* 20, 552–563. doi: 10.1111/faf.12368

Lamarre, E., and Melville, W. K. (1994). Sound-speed measurements near the ocean surface. *J. Acoustical Soc. America* 96, 3605–3616. doi: 10.1121/1.410578

Larayedh, R., Cornuelle, B. D., Krokos, G., and Hoteit, I. (2024). Numerical investigation of shipping noise in the Red Sea. *Sci. Rep.* 14, 5851. doi: 10.1038/s41598-024-56523-2

Levenson, C., and Doblar, R. A. (1976). Long-range acoustic propagation through the Gulf Stream. *J. Acoustical Soc. America* 59, 1134–1141. doi: 10.1121/1.380974

Li, J., Li, P., and Chen, S. (2011). "Specifications for oceanographic survey," in *China Standardization*, 34–38. Available at: https://openstd.samr.gov.cn/bzgk/gb/newGbInfo?hcno=D9FCAB4A332AD98631C272214BB3DE11.

Li, S., Li, Z., Li, W., and Yu, Y. (2021). Three-dimensional sound propagation in the south China sea with the presence of seamount. *J. Mar. Sci. Eng.* 9, 1078. doi: 10.3390/jmse9101078

Li, S., Lin, M., Xu, X., Xing, L., Zhang, P., Gozlan, R. E., et al. (2016). First record of the Indo-Pacific humpback dolphins (Sousa chinensis) southwest of Hainan Island, China. *Mar. Biodiversity Records* 9, 1–6. doi: 10.1186/s41200-016-0005-x

Li, M., Tan, K., Huang, J., and Xie, L. (2022). Seasonal variation of water masses and current field in the northeastern Beibu Gulf based on observations in 2018-2019. *J. Mar. Sci. (in Chinese)* 40, 73–85. doi: 10.3969-j.issn.1001-909X.2022.03.007

Lin, Y. T., and Duda, T. F. (2012). A higher-order split-step Fourier parabolic-equation sound propagation solution scheme. *J. Acoustical Soc. America* 132, EL61–EL67. doi: 10.1121/1.4755276

Lin, W., Zheng, R., Liu, B., Chen, S., Lin, M., Liu, M., et al. (2022). Low survivals and rapid demographic decline of a threatened estuarine delphinid. *Front. Mar. Sci.* 9. doi: 10.3389/fmars.2022.782680

Liu, D., Li, Z., Wang, G., and Liu, Y. (2021). Sound propagation with undulating bottom in shallow water. *J. Mar. Sci. Eng.* 9, 1010. doi: 10.3390/jmse9091010

Liu, Q., and Lu, B. (2008). Seabed sediment acoustic attenuation in shallow seas of the South China sea. *Haiyang Xuebao (in Chinese)* 30, 48–55. Available at: http://www.hyxbocean.cn/article/id/20080406.

Liu, Y., Meng, Z., Chen, Y., and Chen, W. (2023). Analysis of the influence of the continental shelf slope in the South China Sea on sound propagation. *Continental Shelf Res.* 262, 105042. doi: 10.1016/j.csr.2023.105042

Liu, Z., Yang, H., and Wei, X. (2020). Spatiotemporal variation in precipitation during rainy season in Beibu Gulf, South China, from 1961 to 2016. *Water* 12, 1170. doi: 10.3390/w12041170

Lunkov, A., Sidorov, D., and Petnikov, V. (2021). Horizontal refraction of acoustic waves in shallow-water waveguides due to an inhomogeneous bottom structure. *J. Mar. Sci. Eng.* 9, 1269. doi: 10.3390/jmse9111269

Mellberg, L. E., Robinson, A. R., and Botseas, G. (1990). Modeled time variability of acoustic propagation through a Gulf Stream meander and eddies. *J. Acoustical Soc. America* 87, 1044–1054. doi: 10.1121/1.398831

Popper, A. N., and Hawkins, A. D. (2019). An overview of fish bioacoustics and the impacts of anthropogenic sounds on fishes. *J. fish Biol.* 94, 692–713. doi: 10.1111/jfb.13948

Porter, M. B. (1992). *The KRAKEN Normal Mode Program* (Washington, DC: Naval Research Laboratory). Available at: https://openlibrary.cmre.nato.int/handle/20.500.12489/201?show=full (Accessed September 01, 2023).

Porter, M. B. (2011). *The bellhop manual and user's guide: Preliminary draft* Vol. 260 (La Jolla, CA, USA: Heat, Light, and Sound Research, Inc.). Available at: http://oalib.hlsresearch.com/Rays/HLS-2010-1.pdf. Tech. Rep (Accessed September 01, 2023).

Porter, M. B. (2019). Beam tracing for two-and three-dimensional problems in ocean acoustics. *J. Acoustical Soc. America* 146, 2016–2029. doi: 10.1121/1.5125262

Santos-Domínguez, D., Torres-Guijarro, S., Cardenal-López, A., and Pena-Gimenez, A. (2016). ShipsEar: An underwater vessel noise database. *Appl. Acoustics* 113, 64–69. doi: 10.1016/j.apacoust.2016.06.008

Siderius, M., and Porter, M. B. (2008). Modeling broadband ocean acoustic transmissions with time-varying sea surfaces. *J. Acoustical Soc. America* 124, 137–150. doi: 10.1121/1.2920959

Soloviev, A., Gilman, M., Young, K., Brusch, S., and Lehner, S. (2009). Sonar measurements in ship wakes simultaneous with TerraSAR-X overpasses. *IEEE Trans. Geosci. Remote Sens.* 48, 841–851. doi: 10.1109/TGRS.2009.2032053

Spiesberger, J. L., Birdsall, T. G., Metzger, K., Knox, R. A., Spofford, C. W., and Spindel, R. C. (1983). Measurements of Gulf Stream meandering and evidence of seasonal thermocline development using long-range acoustic transmissions. *J. Phys. oceanography* 13, 1836–1846. doi: 10.1175/1520-0485(1983)013<1836:MOGSMA>2.0.CO;2

Wang, Z., Fang, L., Shi, W., Wang, K., and Wang, D. (2013). Whistle characteristics of free-ranging Indo-Pacific humpback dolphins (Sousa chinensis) in Sanniang Bay, China. *J. Acoustical Soc. America* 133, 2479–2489. doi: 10.1121/1.4794390

Wong, G. S., and Zhu, S. M. (1995). Speed of sound in seawater as a function of salinity, temperature, and pressure. *J. Acoustical Soc. America* 97, 1732–1736. doi: 10.1121/1.413048

Wu, S. L., Li, Z. L., and Qin, J. X. (2015). Geoacoustic inversion for bottom parameters in the deep-water area of the South China Sea. *Chin. Phys. Lett.* 32, 124301. doi: 10.1088/0256-307X/32/12/124301

Xia, M., Chen, J., Zhang, P., Peng, P., and Claramunt, C. (2024). Spatial structure and vulnerability of container shipping networks: A case study in the Beibu gulf sea area. *J. Mar. Sci. Eng.* 12, 1307. doi: 10.3390/jmse12081307

Yong, L., Zhang, Y., Zhao, L., Zeng, Q., Lin, L., Gao, M., et al. (2023). Research advances on the ecology of Sousa chinensis. *Biodiversity Sci. (In Chinese)* 31, 22670. doi: 10.17520/biods.2022670

Yu, F., Fan, Z., Hu, H., Zhao, Y., Tang, J., and Chen, G. (2020). A regional parameterisation method for oil spill susceptibility assessment in Beibu Gulf. *Ocean Eng.* 215, 107776. doi: 10.1016/j.oceaneng.2020.107776

Zheng, Q., Zhang, R., Wang, Y., Pan, X., Tang, J., and Zhang, G. (2012). Occurrence and distribution of antibiotics in the Beibu Gulf, China: impacts of river discharge and aquaculture activities. *Mar. Environ. Res.* 78, 26–33. doi: 10.1016/j.marenvres.2012.03.007